Journal of Molecular Modeling (2021) 27: 357
https://doi.org/10.1007/s00894-021-04962-3

ORIGINAL PAPER

Behaviours of antiviral Oseltamivir in different media: DFT and SQMFF calculations

Mohammad Vakili[1] · Elida Romano[2] · Vahidreza Darugar[1] · Silvia Antonia Brandán[2]

Received: 17 August 2021 / Accepted: 20 October 2021 / Published online: 23 November 2021

Abstract

The synthetic cyclohexenecarboxylate ester antiviral Oseltamivir (O) have been theoretically studied by B3LYP/6–311 + + G** calculations to estimate its reactivity and behaviour in gas and aqueous media. The most stable structure obtained in above media is consistent with that reported experimental for Oseltamivir phosphate. The solvation energy value of (O) in aqueous media is between the predicted for antiviral Idoxuridine and Ribavirin. Besides, (O) containing a NH_2 group and NH group reveals lower solvation energy compared with other antiviral agents with an NH_2 group, such as Ribavirin, Cidofovir, and Brincidofovir. Atomic charges on N and O atoms in acceptors and donor groups reveal different behaviours in both media, while the natural bond orbital (NBO) studies show a raised stability of (O) in aqueous solution. This latter resulted is in concordance with the lower reactivity evidenced in water. Frontier orbital studies have revealed that (O) in gas phase has a very similar gap value to antiviral Cidofovir used against the e*bola* disease, while Chloroquine in the two media are more reactive than (O). This study will allow to identify (O) by using vibrational spectroscopy because the 144 vibration modes expected have been assigned using the harmonic force fields calculated from the scaled mechanical force field methodology (SQMFF). Scaled force constants for (O) in the mentioned media are also reported for first time. Due to hydration of the C = O and NH_2 groups by solvent molecules, the calculations in solution produce variations not only in the IR wavenumbers bands, but also in their intensities.

Keywords Oseltamivir · Structural properties · Force fields · Vibrational study · DFT calculations

Introduction

Chemically, Oseltamivir is a synthetic cyclohexenecarboxylate ester with antiviral activity whose IUPAC name is ethyl (3*R*,4*R*,5*S*)-4-acetamido-5-amino-3-pentan-3-yloxycyclohexene-1-carboxylate [1–19]. Oseltamivir is used in health sciences for the treatment of influenza A and influenza B [5–8]. Lindegårdh et al. have reported the use of HPLC for evaluation of Oseltamivir, while the same technique is used in other study for the determination of Oseltamivir phosphate and generic versions [1, 2]. Spectrofluorimetric and rapid capillary electrophoresis methods are also employed for the determination of Oseltamivir phosphate in capsules and generic versions [3, 4]. The most used method is the vibrational spectroscopy, including the SERS technique, because these methods are fast and highly reliable [9, 11, 15–17]. The quantification of Oseltamivir by Raman spectroscopy and the combination of the SERS technique with functional gold nanoparticles allow rapid identification of the Oseltamivir-resistant H1N1 virus, as was recently published [16, 17]. To assign all vibrational bands, IR and Raman, bands of Oseltamivir, first is necessary to determinate its most stable structure. So far, configurations and conformations of (-)-Oseltamivir using a multi-chiroptical approach [12] and studies in silico on stereoisomers of Oseltamivir [14] were reported, but the vibrational assignments of Oseltamivir are not reported yet. Hence, the objectives here are (i) to analyze the most stable structure of Oseltamivir in gas phase and water, as solvent, at B3LYP level using 6–311 + + G**, as basis set [20, 21]; (ii) to evaluate charges of atoms, electrostatic potentials,

✉ Silvia Antonia Brandán
sbrandan@fbqf.unt.edu.ar

[1] Department of Chemistry, Faculty of Science, Ferdowsi University of Mashhad, Mashhad, Iran

[2] Cátedra de Química General, Instituto de Química Inorgánica, Facultad de Bioquímica. Química Y Farmacia, Universidad Nacional de Tucumán, Ayacucho 471, (4000) San Miguel de Tucuman, Tucumán, Argentina

acceptors-donor interactions, topological properties, reactivity, and behavior of Oseltamivir as an isolated molecule and, then, to compare with the values in solution; and (iii) to use the scaled quantum mechanical force field (SQMFF) methodology and the Molvib, as a Fortran program, to assign the observed bands in its available IR spectrum. To achieve this latter purpose, scaling factors together and definitions of normal internal coordinates are necessary [22–25]. Here, calculations and optimizations in water were performed with the polarized continuum method (PCM) and the universal solvation model [26–28]. Here, the above level of calculations combined with the harmonic force fields is a very good tactic to assign experimental bands to vibration modes [29–33]. To conclude, comparisons of predicted properties for Oseltamivir which reported for antiviral agents are presented because the existence of donors and acceptor groups in the structure is important parameters in a pharmacological drug, as proposed by Veber and Lipinski [32–43].

Material and methods

Configurational and conformational studies of Oseltamivir together with analysis of its stereoisomers were already reported by Górecki and by Hajzer et al. [12, 14], respectively and, for these reasons, in this work, the most stable structure was directly used to optimize Oseltamivir in two phases, gas and water as solvent, at B3LYP/6–311 + + G** level of DFT and the Gaussian program [44]. The optimizations in solution were done with the integral equation-formalism polarizable continuum (IEF-PCM) and universal solvation methods [26–28]. Then, the corrected solvation energy were obtained from the subtract of the energies between soluttgv6ion and gas phase, while the energies due to the non-electrostatic term were obtained from the calculations in solution [44]. The volume changes were obtained with the Moldraw program at the same level of calculations [45]. The natural bond orbital (NBO) and atoms in molecules (AIM) 2000 programs were used to predict different types of interactions, charges, electrostatic potentials, acceptor–donor interactions, and topological properties [46–48]. The molecular electrostatic potentials (MEP) were achieved from atomic Merz-Kollman (MK) charges derived from semiempirical methods [49] while with the *GaussView* program were obtained graphs of mapped surfaces [50]. To analyze possible activities and behaviours of Osetamivir in the aforesaid phases, the differences between the border orbitals, named gap, and some important descriptors calculated from known equations [29–33, 36, 51] were analyzed. Besides, the ^{1}H-, ^{13}C-NMR, and electronic spectra of Oseltamivir in aqueous solution were obtained with the Gauge-Independent Atomic Orbital (GIAO) method and the time-dependent DFT calculations (TD-DFT) [52], respectively. The vibrational study of Oseltamivir was performed in both media with the SQMFF methodology and the Molvib program by using scaling factors and the calculated harmonic force fields [22–25]. In the normal internal coordinate's analysis, the NH_2 and CH_3 groups were considered with C_{2v} and C_{3v} symmetries, respectively, while only potential energy distribution (PED) contributions ≥ 10% were employed in the assignments. Here, the theoretical Raman spectra predicted in above-mentioned media in activities were changed to intensities with convenient equations [53]. All of the mentioned calculations obtained at B3LYP/6–311 + + G** level of DFT.

Results and discussion

Optimizations in gas and aqueous solution

The more stable structure of Oseltamivir was proposed by Marcin Górecki [54] and was optimized in above phase at the above-mentioned level. This structure is shown in Fig. 1, while Table 1 indicates the total energy uncorrected and corrected by zero point vibrational energy (ZPVE), dipole moments, and volumes calculated for Oseltamivir in both media. In that table are also included the permittivity's values of two media. The analyses of results demonstrate that in water the dipole moment value of Oseltamivir increases while a contraction in the volume is observed due to its hydration. The dipole moment vectors are located from centre ring with direction outside as can be seen in the superior graphic of Figure S1, see supplementary materials. The corrected solvation energy value (ΔGc) of Oseltamivir determined at the same level of calculations is shown in Table 2. The predicted value for Oseltamivir (− 127.37 kJ/mol) is most negative (slightly higher) than the antiviral Idoxuridine (− 124.50 kJ/mol) but lower than antiviral Ribavirin (− 141.85 kJ/mol) [40, 41], as observed in Table 3. The latter table shows comparisons between the value of Oseltamivir and other predicted for antiviral agents by the above calculated level of theory. Structures of compared antivirals agents including the corresponding to Oseltamivir are presented in Figure S2, see supplementary material. The different acceptor and donor groups of H bonds justify the different values of solvation energy. The mentioned values are also compared with the corresponding to Oseltamivir phosphate calculated in this work in aqueous solution (− 121.13 kJ/mol). Therefore, Oseltamivir presents lower value than Ribavirin, Cidofovir, and Brincidofovir because this antiviral species has one NH_2 group and one N–H bond, while the other species have only one NH_2 group, but present a greater amount of hydroxyl groups or oxygen with a single NH bond. Figure 2 shows the solvation energy values increase as acceptor and donor groups are added in the

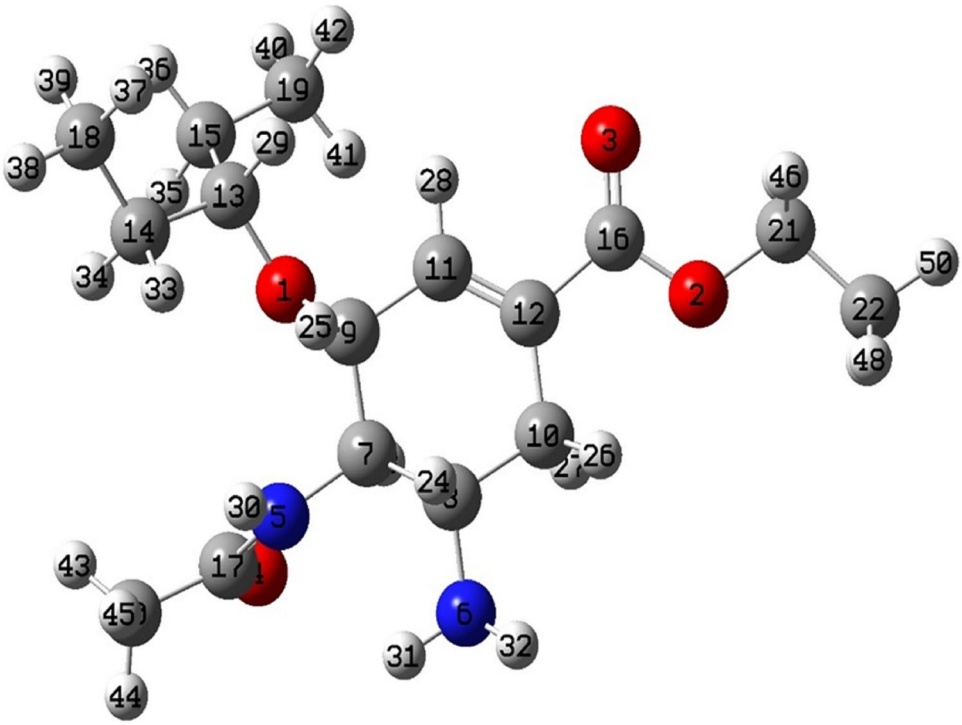

Fig. 1 Molecular structure of the most stable conformer of Oseltamivir and atoms numbering

Table 1 Calculated total and corrected by ZPVE energies (E), dipole moments (μ), and volumes (V) of Oseltamivir in gas phase and aqueous, solutions by using B3LYP/6–311 + + G** level of theory. Permittivity's (ε) values of two media are also included

Oseltamivir					
Medium	E (Hartrees)	E ZPVE	μ (D)	V (Å^3)	ε
Gas	− 1037.2860	− 1036.8534	5.13	353.5	1
Water	− 1037.3206	− 1036.8876	9.63	350.4	78.3553

Table 2 Corrected solvation energy (ΔG_C) in kJ/mol and volumes variations (ΔV) of Oseltamivir in gas phase and aqueous solution

B3LYP/6–311 + + G** method			
$\Delta G_{un}{}^{\#}$	ΔG_{ne}	ΔG_C	ΔV (Å^3)
− 89.71	37.66	− 127.37	− 3.1

$\Delta G_{un}{}^{\#}$ uncorrected, ΔG_{ne} non-electrostatic terms

structures of antiviral agents. Note that the solvation energy value of Oseltamivir is slightly higher than Oseltamivir phosphate.

Geometries in both media

To obtain an accurate vibrational analysis, a good structural study is essential and, hence, the theoretical parameters calculated for Oseltamivir were compared with the experimentally determined for Oseltamivir phosphate [55] by Naumov et al. who determined two cationic structures present in the salt crystal, which they called cation 1 and cation 2. Table 4 indicates the optimized geometry for this compound in two media. Here, to evaluate the optimization achieved, the agreement between the optimized structural parameters with the experimental reported in the literature was considered [55], using the mean square deviation (RMSD) values. It is stated that the bond lengths and bond angles indicate low RMSD values, which determines a good approximation to the proposed structure. The value of RMSD for bond lengths are very small (between 0.0032 and 0.0045 Å); the lowest value is presented in aqueous solution and the best correlation with cation 2, while in gas phase presents better correlation with cation 1. In the case of bond angles values, in both phases present a good correlation with cation 1, showing low RMSD values (between 0.32 and 0.35°). If the dihedral angles are estimated, the lowest RMSD values are 34.09° in PCM compared to cation 2 and 39.60° for gas compared to cation 1. The dihedral angles related to the ethyl groups attached to the tertiary carbon bound to oxygen (C13) present a better correlation with cation 1, whereas the greatest variations are obtained in the dihedral angles involving the carbon atoms of carbonyl group (C16 and C17).

Table 3 Solvation energies (ΔG_C in kJ/mol) and numbers of N–H and O–H groups and N and O atoms present in 13 antiviral species in aqueous solution by using the hybrid B3LYP/6–311 + + G** level of theory

No	Species	ΔG_C	N–H	NH_2	O–H	O	C = O	N	Total	Groups	Rings
1	Isothiazol[b]	− 37.51	1					2	3	SH, C≡N	R5, R6
2	S(−) Chloroquine[c]	− 55.07	1					3	4	Cl	2 R6
	R(+) Chloroquine[c]	− 59.91	1					3	4	Cl	2 R6
3	Niclosamide[d]	− 78.43	1		1	4	1	2	9	2 Cl, NO_2	2 R6
4	Zalcitabine[k]	− 78.92		1	1	3	1	3	9		R5, R6
5	Emtricitabine[e]	− 100.88		1	1	3	1	3	9	F	R5, R6
6	Trifluridine[f]	− 113.85	1		2	5	2	2	12	CF_3	R5, R6
7	Thymidine[f]	− 116.16	1		2	5	2	2	12	CH_3	R5, R6
8	**Oseltamivir phosphate**[a]	− 121.13	1	1	3	8	2	2	17	H_3PO_4	R6
9	Idoxuridine[g,#]	− 124.50	1		2	5	2	2	12	I	R5, R6
10	**Oseltamivir**[a]	**− 127.37**	**1**	**1**		**4**	**2**	**2**	**11**		**R6**
11	Ribavirin[h]	− 141.85		1	3	5	1	4	14		2R5
12	Cidofovir[i]	− 169.21		1	3	6	1	3	14	H_2PO_3	R6
13	Foscarnet[j]	− 219.64			12	5	2		19	3 Na, PO_3	
14	Brincidofovir[i]	− 227.34		1	2	7	1	3	15	HPO_3	R6

[a]This work

[b]From Ref[36]

[c]From Ref[31]

[d]From Ref[32]

[e]From Ref[37]

[f]From Ref[38]

[g]From Ref[39]

[h]From Ref[40]

[i]From Ref[35]

[j]From Ref[41]

[k]From Ref[42]

[#]Idoxuridine calculated by using B3LYP/3-21G* calculations

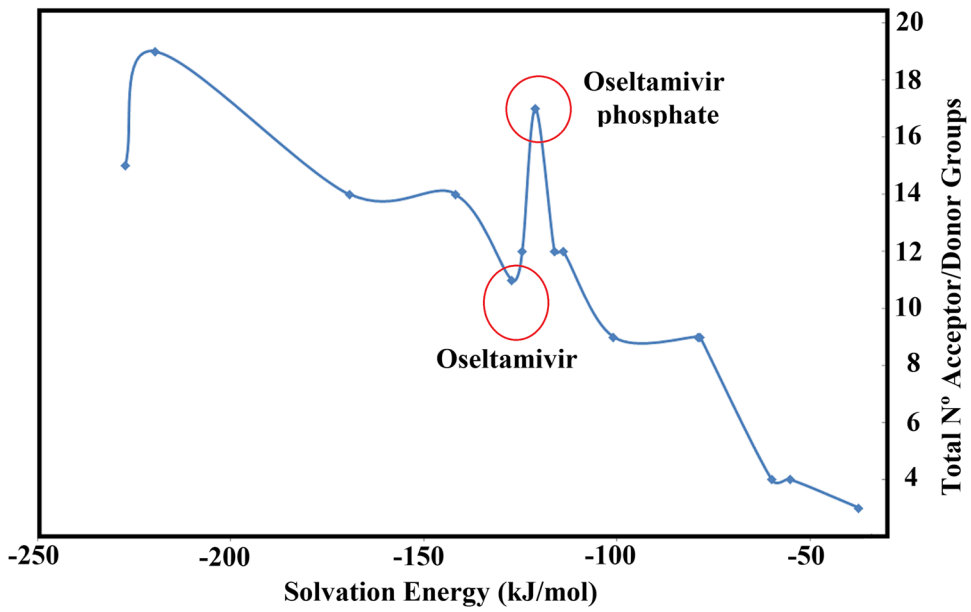

Fig. 2 Total number of acceptor and donor groups of antiviral agents as function of corrected solvation energy values compared with the corresponding to Oseltamivir by using B3LYP/6–311 + + G** level of theory

Charges, electrostatic potential, and bond order studies

To explain the behaviours of species in different media, properties such as the charge of atoms, molecular electrostatic potentials, and bond orders (BO) were determined. The behaviours of species in different media can be analysed by the mentioned parameters. Hence, atomic Merz-Singh-Kollman (MK), Mulliken, and natural population atomic (NPA) charges together with MEP and BO, revealed as Wiberg indices, were obtained for Oseltamivir only on O and N atoms and, in the case of C atoms, only for those attached to nitrogen atoms because these atoms belong to acceptors and donors groups of H bonds. According to analyzing the NPA charges in both media, the most negative value is obtained on the N6 of NH_2 group, while Mulliken charges show the C7 atom with the most negative value, followed by the N6 atom in both media, as shown in Table 5. The full analysis of Table 5 indicates that the charges of O2, O3, and O4 atoms in the both media are negative values and the most negative value is observed for O4 in all cases, but the Mulliken charges on O1 is positive values in both phases. Also, the Mulliken charges on N5 atoms in the mentioned media have positive values, while MK and NPA charges display negative values on this atom in both media. Figure 3 shows the different behaviours of MK (light gray line), NPA (orange line), and Mulliken charges (light blue line) on O, N, and C atoms of Oseltamivir in gas phase. Here, we quickly observed the discrepancy in Mulliken charges on O1 and N5 atoms, previously mentioned. Also, in aqueous solution, the same tendencies are observed.

The MEP values for Osaltimivir in gas and water have been calculated at the similar level and by using the Merz-Singh-Kollman scheme (Table 6). Similar MEP values can be observed in the two media. The molecule's charge distribution can be represented by mapped electrostatic potential surfaces whose colorations determine how molecules interact with each other at reactive sites. These distributions of charges in this compound are very well observed on the mapped surfaces represented with the *GaussView* program [50]. Thus, red, blue, and green colours on the MEP surfaces show respectively different nucleophilic, electrophilic, and inert regions of reactivity (see Fig. 4). Hence, the graphics in both media show the three colours in the same regions. Hence, on free pairs of N and O atoms are observed strong red colours and light blue colours on the H31 and H32 atoms of NH_2 group, on the H30 atom of NH group, and on the H atoms of CH_3 group. Then, nucleophilic sites are characterized by red colour and electrophilic sites by blue colour, while the regions with green colour are inert sites. From these MEP surfaces, we clearly observed that carbonyl group and imino/amino groups are the favourable sites for

Table 4 Comparison of calculated geometrical parameters for the Oseltamivir in gas and water solutions compared with the corresponding experimental ones in the solid phase

B3LYP/6–311 + + G**[a]				
Parameters	Gas	Water	Experimental[b]	
			Cation 1†	Cation 2‡
Bond lengths (Å)				
C17 = O4	1217	1244	1236	1244
C16 = O3	1211	1223	1219	1212
N6-C8	1462	1470	1479	1493
N5-C7	1457	1459	1449	1450
C10-C12	1508	1509	1481	1513
C12 = Cl1	1338	1339	1338	1330
C16-Cl2	1495	1489	1493	1496
C17-N5	1376	1349	1355	1335
C9-O1	1423	1433	1420	1428
C13-O1	1439	1454	1450	1448
C16-O2	1351	1340	1334	1340
C21-O2	1449	1460	1471	1449
RMSD†	**0.0045**	**0.0032**		
RMSD‡	**0.0051**	**0.0030**		
Bond angles (°)				
C17-N5-C7	123.3	125.1	125.0	123.3
N5-C7-C9	110.7	110.3	111.6	110.7
C20-C17-O4	121.7	120.8	122.9	121.6
C20-C17-N5	115.0	116.1	115.5	118.1
N5-C17-O4	123.2	123.1	121.6	120.3
C12-C16-O3	125.4	125.2	123.5	123.9
C9-O1-C13	116.8	115.7	116.4	114.6
C16-O2-C21	116.5	117.8	113.9	115.4
C14-C13-O1	110.3	109.8	110.7	105.5
C15-C13-O1	106.5	106.9	106.5	110.7
C14-C13-C15	113.2	113.6	115.4	113.1
N6-C8-C10	108.5	109.2	110.5	110.9
N6-C8-C7	109.9	110.5	110.5	111.5
Cl0-C12-C11	122.4	122.3	123.3	121.3
Cl0-C8-C7	110.4	110.2	111.4	110.5
C7-C9-C11	112.0	111.8	111.6	110.0
C9-C11-C12	124.4	124.1	123.5	125.9
RMSD†	**0.32**†	**0.35**†		
RMSD‡	**0.53**‡	**0.49**‡		
Dihedral angles (°)				
C7-N5-C17-O4	9.5	0.9	3.2	1.4
C17-N5-C7-C8	124.3	− 114.3	− 126.3	− 102.3
N6-C8-C7-C9	178.2	176.5	174.0	167.5
N6-C8-C7-N5	54.8	53.9	49.9	44.6
N5-C7-C9-O1	− 68.0	− 68.9	− 66.1	− 67.5
O3-C16-O2-C21	− 0.8	− 0.2	4.8	0.5
C15-C13- O1-C9	153.8	152.2	159.5	75.8
C14-C13- O1-C9	− 83.1	− 84.1	− 74.3	− 161.5
C7-N5-C17-C20	− 171.1	− 179.3	− 175.1	− 178.7
C12-C16-O2-C21	179.0	179.2	− 176.9	− 179.2
C16-O2-C21-C22	− 179.4	178.7	− 176.2	172.4
RMSD	**39.60**† **51.10**‡	**45.74**† **34.09**‡		

[a]This work

[b]Ref[54]

reactions of Oseltamivir with electrophil and nucleophil potential biological reactive, respectively.

Natural bond orbital, NBO, and atoms in molecules, AIM studies

To discuss the antiviral property of Oseltamivir, the study of its stability in gas and water are useful and interesting. It related to the presence of N–H, NH_2, and C = O groups containing donor (N–H) and acceptor H bonds (O and N). Thus, intra-molecular interactions can be predicted with the second-order perturbation theory analyses, E^2; were obtained by NBO results and with the topological parameters; and calculated by using the AIM 2000 program [46–48]. Regarding the donor–acceptor interactions of Oseltamivir in both phases, we observed five $\pi \rightarrow \pi^*$, $\sigma \rightarrow \sigma^*$, $n \rightarrow \pi^*$, $n \rightarrow \sigma^*$, and $\pi^* \rightarrow \pi^*$ interactions in the mentioned media, while the $\pi^* \rightarrow \sigma^*$ and $\sigma^* \rightarrow \pi^*$ interactions are respectively observed only in gas and aqueous media (see Table S1, see supplementary materials). Nevertheless, the *LP(1)O3* → *σ*O2-C16* interaction observed in gas phase has a value of 136.06 kJ/mol which decreases to 125.02 kJ/mol in water as solvent, while the value of *LP(1) O4* → *σ*N5-C17* interaction is 105.84 kJ/mol in gas phase

Table 6 Molecular electrostatic potentials (MEP) (a.u.) and bond orders, expressed as Wiberg indexes of antiviral Oseltamivir in two media by using B3LYP/6–311 + + G** level of theory

Atoms	Wiberg Index		MEP	
	Gas	Water	Gas	Water
O1	2008	1981	− 22,366	− 22,367
O2	2150	2166	− 22,325	− 22,324
O3	2017	1959	− 22,389	− 22,392
O4	1995	1874	− 22,414	− 22,422
N5	3219	3272	− 18,367	− 18,363
N6	2823	2800	− 18,414	− 18,411
C7	3930	3934	− 14,728	− 14,727
C8	3962	3956	− 14,730	− 14,729

Table 5 Mulliken, Merz-Kollman, and NPA charges (a.u.) of antiviral Oseltamivir in two media by using B3LYP/6–311 + + G** level of theory

Atoms	MK		Mulliken		NPA	
	gas	Water	Gas	PCM Ely	gas	Water
O1	− 0.065	− 0.062	0.245	0.145	− 0.610	− 0.628
O2	− 0.393	− 0.397	− 0.033	− 0.045	− 0.565	− 0.558
O3	− 0.072	− 0.074	− 0.221	− 0.316	− 0.607	− 0.655
O4	− 0.562	− 0.555	− 0.247	− 0.404	− 0.620	− 0.717
N5	− 0.490	− 0.496	0.101	0.091	− 0.654	− 0.623
N6	− 0.393	− 0.397	− 0.320	− 0.425	− 0.839	− 0.860
C7	− 0.475	− 0.451	− 0.614	− 0.511	− 0.048	− 0.042
C8	0.652	0.654	0.367	0.226	− 0.014	− 0.018

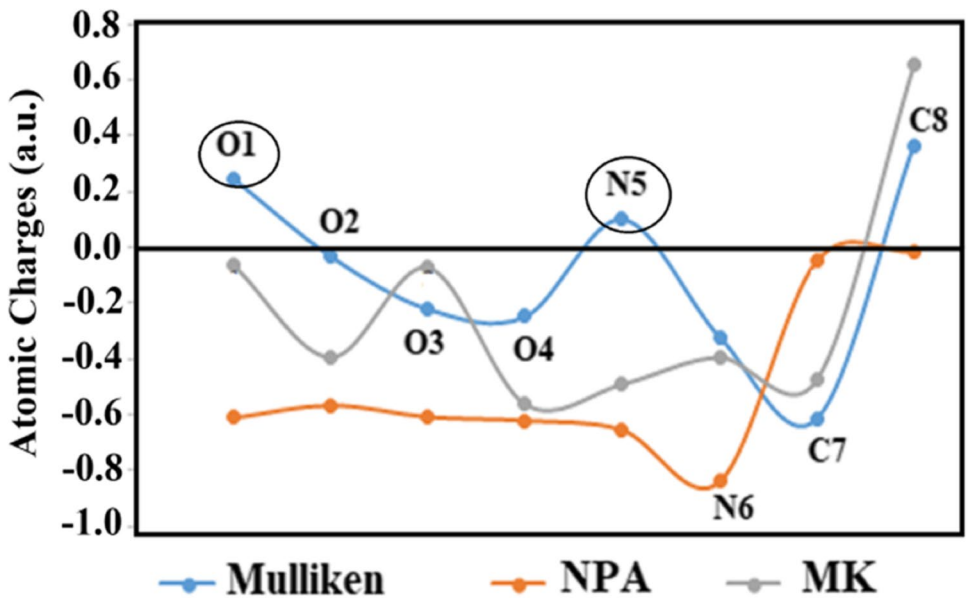

Fig. 3 Variations of MK, atomic Mulliken, and NPA charges on N, O, and C atoms of Oseltamivir in gas phase by using the B3LYP/6–311 + + G** level

which decreases very much in solution to 88.99 kJ/mol. On the contrary, the *LP(1)N5* → *σ*O4-C17* interaction is very weak in gas, 6.10 kJ/mol, while in solution, it increases considerably to 221.79 kJ/mol. Finally, it can be seen that the *σ*O4-C17* → *π*O4-C17* interaction only occurs in solution, while the *π*O4-C17* → *σ*O4-C17* interaction only occurs in the other phase, gas phase. The total energy favours to Oseltamivir in solution (1291.97 kJ/mol) because the value is lower in gas phase (1282.81 kJ/mol). Hence, Oseltamivir in water is more stable than that in gas phase.

The AIM results can be predicted the topological properties in the bond critical points (BCPs) and ring critical points (RCPs). Thus, the electron density, $\rho(r)$; the Laplacian values, $^2\rho(r)$; the eigenvalues ($\lambda1$, $\lambda2$, $\lambda3$) of the Hessian matrix; and the $|\lambda1|/\lambda3$ ratio were calculated for Oseltamivir (Table S2, see supplementary materials). We observed that there are not new bonds or ring critical points formed in the two media. The ionic or highly polar covalent interactions, such as C = O bonds, have $\lambda1/\lambda3 < 1$, while for N–H bonds, $\lambda1/\lambda3 > 1$. On other hand, in all cases, $^2\rho(r) > 0$ (closed-shell interaction) and the eigenvalues of the Hessian matrix have approximately the same values in both media. The molecular graphs of Oseltamivir in gas and aqueous solution show the absence of new critical points (Figure S3, see supplementary materials).

HOMO–LUMO and chemical quantum global descriptors

The differences between HOMO, highest occupied molecular orbital, and LUMO lowest unoccupied molecular orbital are known as gap values that used to guess reactivities, as was suggested by Parr and Pearson [56], while the global descriptors can use to predict the behaviours of molecule too [37–42, 50]. In this study, the HOMO, LUMO, energy band gaps and the chemical potential (μ), electronegativity (χ), global hardness (η), global softness (S), global electrophilicity index (ω), and global nucleophilicity index (E) descriptors [38–43] for Oseltamivir in different media are shown in Table S3, see supplementary materials, together with the equations to compute them. Parameters reported for antiviral species are also presented in the same table. Analyzing Table S3 shows Oseltamivir has a similar gap value (5.2817 eV) to Cidofovir (5.2964 eV) in gas phase. This result is very important taking into account that Cidofovir is an antiviral agent used against the *Ebola* disease. However, Chloroquine in the two media is an antiviral most reactive than Oseltamivir. The gap values generally decrease in solution except for the case of Emtricitabine and Oseltamivir, while the values of global (ω) and (E) for Oseltamivir in water are greater than those in the gas, although the gap value is greater in solution, as observed in Table S3, see supplementary materials, which could suggest higher hydration and low reactivities in the mentioned media. Possibly, the higher solvation energy of Oseltamivir (− 127.37 kJ/mol) and for Chloroquine (− 55.07 kJ/mol and − 59.91 kJ/mol, for S and R, respectively) could be supported by the higher values of ω and E in both medium.

Vibrational study

There are 144 normal modes for the optimized structure of Oseltamivir in aforementioned media with C_1 symmetries. In the normal internal coordinate's analysis, the NH_2 and CH_3 groups were considered with C_{2v} and C_{3v} symmetries, respectively. The reported IR spectrum of Oseltamivir phosphate in the solid phase obtained from Ref. [9] is compared in Fig. 5 with the calculated in two media, while the theoretical Raman spectra for Oseltamivir in the mentioned media are compared in Figure S4, see supplementary materials. The hydration of Oseltamivir in aqueous solution causes a change in the wavenumbers and intensities of IR bands in

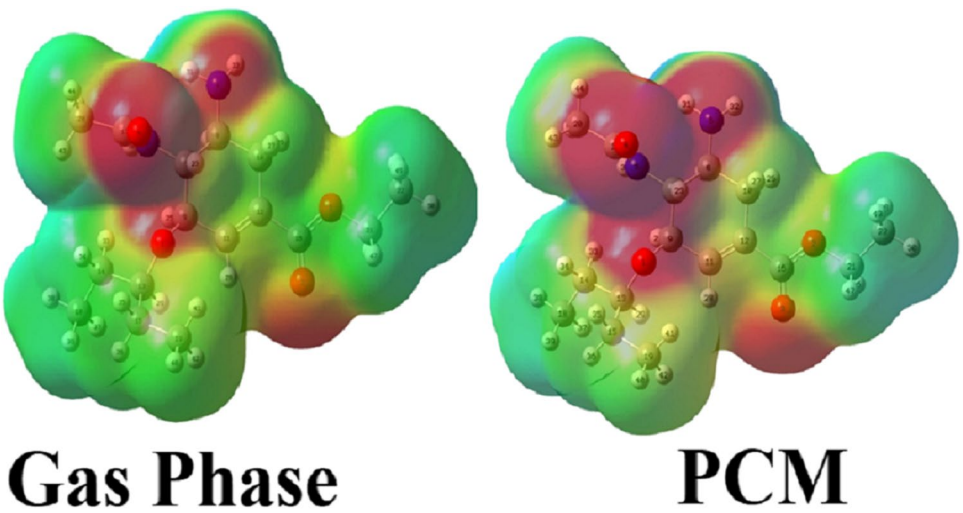

Fig. 4 Calculated electrostatic potential surfaces on the molecular surfaces of Oseltamivir in gas phase (left) and water solution (right) by using the B3LYP/6–311 + + G** level. Color ranges ± 0.0463 a.u. Isodensity value of 0.004a.u

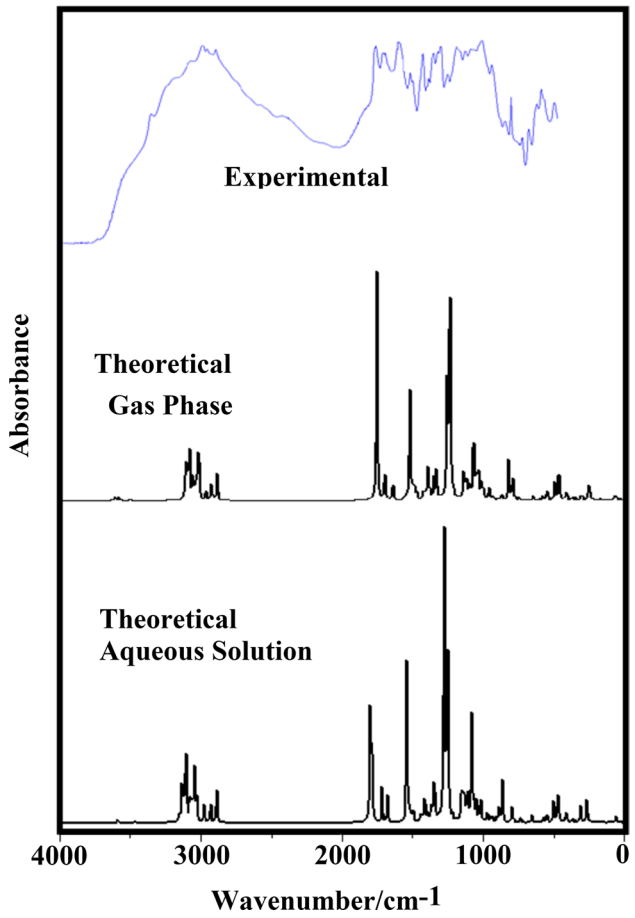

Fig. 5 Comparison of experimental infrared spectra of oseltamivir phosphate in solid phase [9] with the corresponding to oseltamivir in gas phase and aqueous solution by using the hybrid B3LYP/6–311 + + G** method

the 4000–2500 and 2000–10 cm^{-1} regions (see Figure S5, see supplementary materials). Full vibrational assignments for Oseltamivir in both media were done with the SQMFF approach and the Molvib program and, considering the normal internal coordinates and the corresponding harmonic force fields calculated [22, 25]. In this study, the suggested scale factors were used and only potential energy distribution contributions (PED) > 10% were taken into account [23, 24]. Table 7 presents a comparison between the observed wavenumbers with those calculated for Oseltamivir. Some of the most important vibrational band assignments were discussed by regions, see below.

Vibrational band assignments

4000–2000 cm^{-1} region In this region, the NH and CH stretching modes are expected [29–32, 37–41]. First, the weak intensity IR band at 3347 cm^{-1} is attributed to NH stretching mode; its calculated wavenumber obtained at 3460 and 3440 cm^{-1} in gas and aqueous solution, respectively. The IR shoulders at 3227 cm^{-1} and 3172 cm^{-1} are assigned to the antisymmetric and symmetric stretching modes of NH_2, respectively. The calculated NH_2 antisymmetric vibrations are obtained by SQM results at 3437 cm^{-1} in gas and at 3404 cm^{-1} in solution, while their symmetric movement are calculated at 3361 and 3339 cm^{-1}, respectively. The calculated CH_3 and CH_2 antisymmetric vibrations are between 2994 and 2924 cm^{-1}, while their symmetric movements are between 2914 and 2894 cm^{-1}. The shoulder IR band at 2993 cm^{-1} and the very strong intensity IR band at 2977 cm^{-1} are assigned to CH_3 antisymmetric vibration modes. The very strong intensity IR band at 2941 cm^{-1} is assigned to the CH_2 antisymmetric stretching, while the shoulder at 2913 cm^{-1} is attributed to the symmetric stretching of methyl group. The very intensity IR band at 2877 cm^{-1} and the broad and strong intensity band at 2567 cm^{-1} are assigned to the C-H stretching modes. Their calculated bands are predicted between 2846 and 2771 cm^{-1} in gas and 2883 and 2847 cm^{-1} in aqueous solution.

1800–800 cm^{-1} region In this region, the C = O and C = C stretching vibrations are expected [31, 36, 38, 40, 41]. The very strong intensity band at 1715 cm^{-1} and two strong intensity bands at 1663 cm^{-1} and 1651 cm^{-1} are attributed to them. According to SQM results, the C = O stretching obtained at 1698 cm^{-1} and 1697 cm^{-1} in gas and at 1590 cm^{-1} and 1573 cm^{-1} in solution, while the calculated C = C stretching mode belonging to the ring is observed at 1637 and 1644 cm^{-1} in gas and solution, respectively. In addition, the deformation, wagging, and rocking modes of NH_2, CH_3, CH_2, and C-H groups appear in this region [36, 37, 41, 59]. In consequence, the very strong intensity band at 1549 cm^{-1} is attributed to NH_2 deformation mode, δNH_2, and its calculated values by SQM remarked at 1572 and 1535 cm^{-1} in gas and solution, respectively. The very strong intensity IR band at 1535 cm^{-1} is assigned to ρH30-N5 in gas phase and to C17-N5 stretching in solutions, which are predicted at 1506 cm^{-1} and 1512 cm^{-1}. The CH_2 deformation modes and CH_3 antisymmetric deformations, $\delta_a CH_3$, modes are observed between 1453 and 1408 cm^{-1} in gas and between 1434 cm^{-1} and 1394 cm^{-1} in solution. The symmetric deformations of CH_3, $\delta_s CH_3$, are obtained between 1353 and 1337 cm^{-1} in gas phase and between 1348 and 1338 cm^{-1} in solution. The very strong IR band at 1243 cm^{-1} is assigned to rocking mode of NH_2, ρNH_2. In both phases, the calculation wavenumbers of wagging and rocking movements are obtained between 1390/1278 in gas and 1387/1276 cm^{-1} in solution (see Table 7 for their details). The SQM results that obtained the calculated ρCH rocking modes were obtained between 1332 and 1235 cm^{-1} by SQM results. According to calculation results, the strong intensity IR band at 1063 cm^{-1} is assigned to C-N

Table 7 Observed and calculated wavenumbers (cm^{-1}) and assignments for Oseltamivir in gas phase by using the hybrid B3LYP method

Experimental		B3LYP/6–311 + + G** Method			
IR	Int	GAS		PCM	
		SQM[c]	Assignments[a]	SQM[d]	Assignments[a]
3347w	10.8	3460	νN5-H30	3440	νN5-H30
3227sh	4.3	3437	ν_aNH_2	3404	ν_aNH_2
3172sh	1.3	3361	ν_sNH_2	3339	ν_sNH_2
3064sh	1.9	3045	νC11-H28	3048	νC11-H28
2993sh	8.9	2994	ν_aCH_3(C20)	3003	ν_aCH_3(C20)
	36.7	2986	ν_aCH_3(C22)	2995	ν_aCH_2(C21)
	31.7	2982	ν_aCH_3(C19)	2984	ν_aCH_3(C20)
	13.5	2978	ν_aCH_3(C20)	2977	ν_aCH_3(C22)
2977vs	27.7	2974	ν_aCH_3(C22)	2972	ν_aCH_3(C22)
	34.9	2966	ν_aCH_3(C18)	2970	νC7-H23
	7.6	2964	νC7-H23	2966	ν_aCH_3(C19)
	1.8	2960	ν_aCH_2(C21)	2963	ν_aCH_3(C18)
	63.9	2956	ν_aCH_3(C18)	2955	ν_aCH_3(C18)
	28.3	2955	ν_aCH_3(C19)	2954	ν_aCH_3(C19)
	16.8	2937	ν_aCH_2(C10)	2945	ν_aCH_2(C10)
2941vs	20.0	2935	ν_aCH_2(C15)	2940	ν_sCH_2(C21)
	16.0	2927	ν_sCH_2(C21)	2939	ν_aCH_2(C15)
	15.6	2924	ν_aCH_2(C14)	2929	ν_aCH_2(C14)
	9.9	2914	ν_sCH_3(C20)	2922	ν_sCH_3(C20)
2913sh	19.5	2911	ν_sCH_3(C22)	2912	ν_sCH_3(C22)
	10.8	2903	ν_sCH_2(C10)	2900	ν_sCH_2(C15)
	38.0	2902	ν_sCH_2(C15)	2899	ν_sCH_2(C10)
	15.6	2900	ν_sCH_3(C19)	2899	ν_sCH_3(C19)
	24.8	2898	ν_sCH_3(C18)	2898	ν_sCH_3(C18)
	37.2	2894	ν_sCH_2(C14)	2894	ν_sCH_2(C14)
2877vs	25.6	2846	νC13-H29	2883	νC9-H25
	35.7	2805	νC9-H25	2875	νC13-H29
2567 s,br	56.1	2771	νC8-H24	2847	νC8-H24
1715vs	180.2	1698	νC16 = O3	1644	νC11 = C12
1663 s	261.3	1697	νC17 = O4	1590	νC16 = O3
1651 s	74.1	1637	νC11 = C12	1573	νC17 = O4
1549vs	47.8	1572	δNH_2	1535	δNH_2
1535vs	260.3	1506	ρH30-N5	1512	νC17-N5
1464 m	5.22	1453	δCH_2(C21)	1434	δCH_2(C21)
1446w	8.8	1446	δ_aCH_3(C19)	1430	δ_aCH_3(C18)
	8.6	1444	δ_aCH_3(C18)	1426	δ_aCH_3(C19)
	6.3	1438	δ_aCH_3(C18)	1421	δ_aCH_3(C18)
1432sh	4.2	1434	δ_aCH_3(C22)	1413	δ_aCH_3(C19)
1432sh	8.5	1433	δ_aCH_3(C19)	1412	δ_aCH_3(C20)
1432sh	0.6	1427	δ_aCH_3(C20)	1411	δ_aCH_3(C22)
1426sh	9.6	1425	δCH_2(C14)	1408	δCH_2(C14)
	7.1	1423	δ_aCH_3(C22)	1407	δ_aCH_3(C22)
	6.2	1420	δCH_2(C10)	1401	δCH_2(C10)
1406sh	1.6	1412	δCH_2(C15)	1398	δ_aCH_3(C20)
1399sh	11.3	1408	δ_aCH_3(C20)	1394	δCH_2(C15)
1388sh	7.5	1390	ρ′C8-H24	1387	ρ′C8-H24
1372 s	6.1	1378	ρCH_2(C21)	1373	ρC13-H29
1372 s	5.3	1376	ρC13-H29	1370	ρCH_2(C21)

Table 7 (continued)

Experimental		B3LYP/6–311 + + G** Method			
IR	Int	GAS		PCM	
		SQM[c]	Assignments[a]	SQM[d]	Assignments[a]
1366sh	2.4	1362	wagCH_2(C10)	1366	ρC8-H24
1360sh	7.0	1358	ρCH_2(C15)	1357	ρCH_2(C15) ρ′C13-H29
	9.1	1353	$\delta_s CH_3$(C18)	1348	$\delta_s CH_3$(C18)
	48.3	1349	$\delta_s CH_3$(C19)	1346	$\delta_s CH_3$(C22)
1342sh	2.6	1347	$\delta_s CH_3$(C22)	1345	$\delta_s CH_3$(C22)ρC7-H23
1342sh	6.5	1345	ρC9-H25βC11-H28	1340	νC10-C12
1330w	14.5	1337	$\delta_s CH_3$(C20)	1338	$\delta_s CH_3$(C19)
1330w	1.1	1332	ρC8-H24ρC7-H23	1331	$\delta_s CH_3$(C20)
1314sh	35.2	1321	ρC9-H25	1320	ρC9-H25ρC7-H23
1310sh	7.9	1312	wagCH_2(C14)	1309	wagCH_2(C14)
1295 s	55.5	1302	ρCH_2(C14)	1305	ρCH_2(C14)
1285sh	6.3	1294	ρ′C9-H25	1297	ρ′C9-H25
1268sh	2.2	1287	wagCH_2(C15)	1281	wagCH_2(C15)
1261 s	2.5	1278	wagCH_2(C21)	1276	wagCH_2(C21)
1253sh	0.9	1274	βC11-H28	1275	βC11-H28 wagCH_2(C10)
1243vs	4.1	1245	ρ′C7-H23	1258	νC17-N5ρN5-H30
1243vs	9.8	1237	ρ′C13-H29	1241	ρ′C7-H23
1243vs	271.8	1233	ρNH_2	1236	ρNH_2
1191 m	140.1	1215	νC17-N5	1235	ρ′C7-H23 ρ′C13-H29
1191 m	473.9	1207	νC16-O2 νC12-C16	1197	ρCH_2(C10) νC12-C16
1181sh	14.2	1189	ρCH_2(C10)	1182	νC16-O2
1141sh	1.5	1138	ρ′CH_3(C19)	1137	ρ′CH_3(C19)
1125vs	3.5	1118	νC7-C9	1119	νC7-C9
1113sh	11.1	1108	νC13-C14	1107	νC13-C14
	49.5	1105	ρCH_3(C22)	1103	ρCH_3(C22)
	15.8	1103	ρ′CH_3(C18) νC13-C14	1098	βR_1(A1)
1095sh	17.1	1100	ρ′CH_3(C22)	1095	ρ′CH_3(C22)
1077sh	7.3	1090	ρCH_3(C19)	1084	ρCH_3(C19)
1063 s	36.3	1080	νC7-N5 νC7-C8 νC8-N6	1080	νC7-N5 νC7-C8ν C8-N6
1053sh	43.3	1058	νC9-O1	1052	τR_1(A1)
1024 s	180.4	1032	νC9-O1 νC13-O1	1034	ρCH_3(C20)
	36.5	1025	ρCH_3(C20)	1024	νC9-O1νC7-C9
1024 s	3.6	1023	νC9-C11	1022	νC9-C11
1024 s	24.8	1011	νC14-C18 νC15-C19	1012	νC14-C18 νC13-C15
990 s	36.3	1005	νC14-C18 νC13-C14	1003	νC15-C19 νC9-O1
990 s	16.6	998	νC15-C19	999	νC15-C19
990 s	14.3	989	νC21-C22	989	νC21-C22 νC21-O2
	14.8	987	ρCH_3(C18)	986	ρCH_3(C18)
972 s	34.7	976	νC8-C10	978	νC21-C22
960sh	5.9	961	ρ′CH_3(C20)	968	νC9-O1 νC8-C10
944vs	30.7	936	γC11-H28	937	γC11-H28 νC17-C20
912sh	5.5	910	νC17-C20	919	γC11-H28
894sh	1.8	907	γC11-H28	909	ρ′CH_3(C18)
880sh	7.0	901	νC15-C19 ρ′CH_3(C18)	898	νC13-O1
870 m	5.8	876	νC10-C12	888	wagNH_2
850sh	1.8	853	νC21-O2	857	wagNH_2
842sh	4.5	846	ρ′CH_3(C18)	848	νC21-O2
835sh	6.7	835	τwCH_2(C10)	847	τwCH_2(C10)

Table 7 (continued)

Experimental		B3LYP/6–311 + + G** Method			
IR	Int	GAS		PCM	
		SQM[c]	Assignments[a]	SQM[d]	Assignments[a]
773w	73.5	802	$wagNH_2$	836	τwCH_2(C10)
773w	1.8	785	βR_1(A1)	785	wagC16 = O2
729 s	38.3	759	τwCH_2(C21)	769	τwCH_2(C21)
729 s	6.5	733	wagC16 = O2	733	wagC16 = O2τwCH_2(C10)
721sh	0.4	717	τwCH_2(C15)	719	τwCH_2(C14)
650w	9.5	710	τwCH_2(C14)νC13-C15	708	τwCH_2(C15)
639sh	9.2	638	νC17-C20	640	wagN5-C17
602w	0.5	618	wagN5-C17	637	wagN5-C17
588sh	2.1	586	δC7C8N6	588	δC7C8N6
572sh	9.1	571	ρN5-C17	573	ρN5-C17
540 m	13.4	545	δC10C8N6	550	δC10C8N6
540 m	5.0	535	δC15C13O1βR_2(A1)	542	δC15C13O1
509 m	32.4	494	βR_3(A1)	509	wagN5-H30
477sh	41.4	464	wagN5-H30	484	βR_3(A1)δN5C17C20
455sh	32.6	457	δC14C13O1	462	δC14C13O1δC13C15C19 δC14C13C15
432sh	4.8	444	δC7C8N6	445	δC13O1C9
425sh	4.6	416	δO2C16C12	424	δO2C21C22 δO2C16C12
413 m	3.9	408	δN5C17C20	414	βR_2(A1)
397sh	14.1	405	γC12-C16	403	γC12-C16τR_1(A1)
	1.4	375	δO2C21C22	378	δC8C7N5
	7.1	361	ρC16 = O2	361	γC12-C16 ρC16 = O2
	5.0	337	δC9C7N5	337	δC9C7N5
	0.9	303	δC13C15C19	310	δC13C15C19τC17-N5
	13.7	300	δC7C8N6	308	δC7C8N6
	1.5	254	δC13C14C18 δC13O1C9	260	δC13C14C18
	26.6	249	δC21O2C16βC12-C16	254	δC21O2C16βC12-C16
	4.8	233	$\tau_w CH_3$(C22)	246	$\tau_w CH_3$(C22)
	12.3	233	τwNH_2 δN5C17C20	237	τwNH_2
	1.7	222	$\tau wNH_2\tau_w CH_3$(C18)	235	$\tau_w CH_3$(C18) βR_3(A1)
	2.2	208	τwNH_2	222	$\tau_w CH_3$(C18)
	0.8	196	$\tau_w CH_3$(C19)	209	$\tau_w CH_3$(C19)
	1.5	176	$\tau_w CH_3$(C18) δC14C13C15	187	$\tau_w CH_3$(C18)δC14C13C15
	1.8	169	δC7N5C17	175	ρN5-H30
	2.5	145	τR_1(A1)	152	τC14-C13$\tau_w CH_3$(C20)
	0.2	131	τR_2(A1)	145	$\tau_w CH_3$(C20)
	1.2	108	δC8C7N5δC10C8N6	139	τR_2(A1)
	0.0	94	τO2-C16	120	τC14-C13
	0.3	90	τC14-C13	110	τC21-O2
	0.2	86	τC15-C13	102	τC21-O2
	0.4	70	$\tau_w CH_3$(C20)	91	τO2-C16
	0.8	68	τC21-O2	86	δC10C8N6
	6.2	60	τC17-N5τC14-C13	72	τC15-C13
	6.2	55	τC17-N5	64	τC17-N5
	0.8	45	τN5-C7	54	τN5-C7
	0.6	36	τC13-O1	45	τwC16-C12τN5-C7
	1.8	29	τR_3(A1)	32	τC13-O1τR_3(A1)
	1.8	24	τwC16-C12	28	τwC16-C12

Table 7 (continued)

Experimental		B3LYP/6–311 + + G** Method			
IR	Int	GAS		PCM	
		SQM[c]	Assignments[a]	SQM[d]	Assignments[a]
	0.0	19	τO1-C9	23	τO1-C9

Abbreviations: ν stretching, β deformation in the plane, γ deformation out of plane, *wag* wagging, τtorsion, ρ rocking, *Tw* twisting, δ deformation, *a* antisymmetric, *s* symmetric

[a]This work

[b]From scaled quantum mechanics force field with B3LYP/6–311 + + G** method

[c]From scaled quantum mechanics force field with B3LYP/6-31G* method

[d]From B3LYP/6-31G* method,

stretching; its calculated band was obtained at 1080 cm^{-1} in both phases. In relation to C-O stretching, the C16-O2 stretching wavenumber is obtained at higher wavenumbers than of other ones, perhaps because the C16 belongs to the C16 = O3 group. This band is obtained at 1207 cm^{-1} in the gas and at 1182 cm^{-1} in water, while for the other C-O bonds are observed at 1058, 1032, and 853 cm^{-1} in gas and 1024, 898, and 848 cm^{-1} in solution. However, the experimental IR band at 1191 cm^{-1} assigned to C16-O2 stretching and the signals at 1053, 1024, 880, 850, and 842 cm^{-1} are attributed to other C-O stretching modes (see Table 7).

Skeletal modes The very intense IR signal at 1125 cm^{-1} is assigned to C7-C9 stretching, which its calculated wavenumbers in gas and water is 1118 and 1119 cm^{-1}, respectively. The strong intensity IR band at 1024 cm^{-1} was assigned to C9-C11 stretching, as was predicted by the calculations at 1023 cm^{-1} in gas and at 1022 cm^{-1} in water. According to calculated results, other C–C stretching modes are predicted in different positions; thus, the strong and medium intensity IR bands at 972 and 870 cm^{-1} are assigned to these modes, respectively, because the calculations predict these movements at 976 and 876 cm^{-1} in gas phase, while in solution, these modes appear coupling, as can be seen in Table 7. Here, the deformations and torsions rings are predicted with strong coupling among them from 1100 cm^{-1} towards the lower wavenumbers region, as observed in Table 7.

Table 8 Scaled internal force constants for Oseltamivir in gas and water phases by using the B3LYP/6–311 + + G** method

Force constants	Oseltamivir[a]	
	Gas	PCM
$f(\nu N\text{-}H)$	6.64	6.56
$f(\nu NH_2)$	6.42	6.32
$f(\nu CH_3)$	4.80	4.80
$f(\nu CH_2)_{ring}$	4.71	4.71
$f(\nu CH_2)$	4.72	4.75
$f(\nu CH)_{ring}$	4.64	4.76
$f(\nu CH)$	4.48	4.58
$f(\nu C=O)$	11.48	9.87
$f(\nu C=C)$	8.59	8.49
$f(\nu C\text{-}O)$	4.62	4.39
$f(\nu N\text{-}C)$	5.04	5.28
$f(\delta NH_2)$	0.84	0.83
$f(\delta CH_2)$	0.75	0.73
$f(\delta CH_3)$	0.53	0.52
$f\beta_R$	0.21	0.21

Units are mdyn $Å^{-1}$ for stretching and mdyn Å rad^{-2} for angle deformations

[a]This work

Force constants

For Oseltamivir in two studied media, the scaled force constants were obtained at above level of theory with the harmonic force fields calculated with the SQMFF methodology [22–24] and Molvib program [25]. These harmonic force constants for Oseltamivir in both media are presented in Table 8. According to this Table, the $f(\nu C=O)$ decreases considerably in solution. This can be justified due to the increased distance of this bond in aqueous solution. Also, the $f(\nu N\text{-}H)$ and $f(\nu NH_2)$ decreases slightly in solution in comparison with value in gas phase, while the $f(\nu N\text{-}C)$ increases. Finally, the other force constants present approximately the same values, while the deformation force constants unchanged in both media. Table 9 shows a comparison of the some values of force constants for Oseltamivir with reported for compounds containing similar groups. This table shows, for all cases, the $f(\nu C=O)$ in gas phase are similar, but in solution, these values decrease irregularly due to the solvation of these groups, while for the other force constants, similar values are observed.

Table 9 Scaled internal force constants for Oseltamivir in gas and water phases compared with reported for others antivirals by using the B3LYP/6–311 + + G** method

Force constants	Oseltamivir[a]		Rivabirin (C5)[b]		Emtricitabine (C6)[c]		Zalzitabine(C2)[d]		Thymidine(C3)[e]	
	Gas	PCM	Gas	PCM	Gas	PCM	Gas	PCM	Gas	PCM
f(νN-H)	6.64	6.56	-	-	-	-	-	-	6.62	6.49
$f(\nu NH_2)$	6.42	6.32	6.83	6.72	6.88	6.80	6.82	6.74	-	-
f(νC = O)	11.48	9.87	11.88	10.41	11.22	9.81	11.45	9.99	11.63	10.50
f(νC = C)	8.59	8.49	-	-	8.07	8.14	7.97	8.07	8.17	8.09
f(νC-O)	4.62	4.39	4.67	4.96	4.54	4.97	4.47	4.27	4.48	4.26
f(νN-C)	5.04	5.28	6.93	6.81	6.05	6.10	6.01	6.09	5.38	5.45

Units are mdyn $Å^{-1}$ for stretching

[a]This work

[b]From Ref[40]

[c]From Ref[37]

[d]From Ref[42]

[e]From Ref[38]

Conclusions

In this study, the optimized structure and vibrational infrared of synthetic cyclohexenecarboxylate ester antiviral Oseltamivir (O) in gas phase and aqueous solution were elucidate by using B3LYP/6–311 + + G** level of DFT. The optimized most stable theoretical structures determined in both media show very excellent agreement with those experimental reported for Oseltamivir phosphate. The solvation energy value of (O) in water (− 127.37 kJ/mol) is between the predicted for antiviral Idoxuridine (− 124.50 kJ/mol) and Ribavirin (− 141.85 kJ/mol), and it is slightly higher than Oseltamivir phosphate. Besides, (O) containing a NH_2 group and a NH group reveals lower solvation energy as compared with other antiviral agents with an NH_2 group, such as Ribavirin, Cidofovir and Brincidofovir. Atomic MK, NPA, and Mulliken charges reveal different behaviours on the N and O atoms of acceptors and donor groups in both gas and water media, while the NBO results show higher stability of (O) in solution due to five types of donor–acceptor interactions observed in this medium. This latter resulted agrees with lower reactivity evidenced in solution. The frontier orbital studies have revealed that (O) in gas phase has a very similar gap value to antiviral Cidofovir used against the e*bola* disease, while Chloroquine in the two media are most reactive than (O). Now, Oseltamivir can be easily identified by using vibrational spectroscopy because the assignments of 144 vibration normal modes have been done using the harmonic force fields calculated with the SQMFF procedure. Scaled force constants for (O) in the mentioned media are also reported for first time. The calculations in solution predicted shifting of IR bands due to vibration modes of C = O and NH_2 groups as a result of hydration of these groups with water molecules. Besides, the mapped electrostatic potential surfaces have evidenced that carbonyl group and imino/amino groups are the favourable sites for reactions of Oseltamivir with electrophil and nucleophil potentials biological reactive. Hence, knowing these reaction sites in the future, molecular docking calculations could be carried out to investigate antiviral properties by using structures of COVID-19: 6LU7, 6M03, 6W63, and 7BTF.

Supplementary Information The online version contains supplementary material available at https://doi.org/10.1007/s00894-021-04962-3.

Acknowledgements The author would like to thank Prof. Tom Sundius for his permission to use MOLVIB.

Author contribution Mohammad Vakili: Formal analysis and investigation, Elida Romano: Conceptualization, Methodology, Vahidreza Darugar: Conceptualization, Methodology, Silvia Antonia Brandán: Writing, original draft preparation, review, editing and Supervision.

Funding This work was supported with grants from CIUNT Project No. 26/D608 (Consejo de Investigaciones, Universidad Nacional de Tucumán).

Data availability Available when the authors require it.

Code availability Not applicable.

Declarations

Conflict of interest The authors declare no competing interests.

References

1. Lindegårdh N, Hien TT, Farrar J, Singhasivanon P, White NP, Day NPJ (2006) A simple and rapid liquid chromatographic assay for

evaluation of potentially counterfeit Tamiflu®. J Pharm Biomed Anal 42(4):430–433
2. Joseph-Charles J, Geneste C, Laborde-Kummer E, Gheyouche R, Boudis H, Dubost J-P (2007) Development and validation of a rapid HPLC method for the determination of Oseltamivir phosphate in Tamiflu® and generic versions. J Pharm Biomed Anal 44:1008–1013
3. Aydoğmuş Z (2009) Simple and sensitive spectrofluorimetric method for the determination of Oseltamivir phosphate in capsules through derivatization with fluorescamine. J Fluoresc 19:673–679
4. Laborde-Kummer E, Gaudin K, Joseph-Charles J, Gheyouche R, Boudis H, Dubost J-P (2009) Development and validation of a rapid capillary electrophoresis method for the determination of Oseltamivir phosphate in Tamiflu® and generic versions. J Pharm Biomed Anal 50:544–546
5. Dharan NJ, Gubareva LV, Meyer JJ, Okomo-Adhiambo M, McClinton RC, Marshall SA, St George K, Epperson S, Brammer L, Klimov AI, Bresee JS, Fry AM (2009) Infections with Oseltamivir-Resistant Influenza A(H1N1) virus in the United States. J A Med Assoc 301:1034–1041
6. Moscona A (2009) Global Transmission of Oseltamivir-resistant influenza. N Engl J Med 360:953–956
7. Hurt AC (2010) Nor'e SS, McCaw JM, Fryer HR, Mosse J, McLean AR, Barr IG, Assessing the viral fitness of Oseltamivir-resistant influenza viruses in ferrets, using a competitive-mixtures Model. J Virol 84:9427–9438
8. Duan S, Boltz DA, Seiler P, Li J, Bragstad K, Nielse LP, Webby RJ, Webster RG, Govorkova EA (2010) Oseltamivir-resistant pandemic H1N1/2009 influenza virus possesses lower transmissibility and fitness in ferrets. PLoS Pathog. 6:e1001022
9. Bunaciu AA, Nita S, Fleschin Ş, Aydoğmuş Z, Aboul-Enein HY (2012) A Fourier transform infrared spectrophotometry method used for Oseltamivir determination in pharmaceutical formulations. GU J Sci 25(3):631–634
10. Vishkaee TS, Mohajerani N, Nafisi S (2013) A comparative study of the interaction of Tamiflu and Oseltamivir carboxylate with bovine serum albumin. J Photochem Photobiol, B 119(5):65–70
11. Siddiqui A, Shah RB, Khan MA (2013) Oseltamivir phosphate–amberlite^{TM} IRP 64 ionic complex for taste masking: preparation and chemometric evaluation. J Pharmaceutical Sciences 102(6):1800–1812
12. Górecki M (2015) Configurational and conformational study of (-)-Oseltamivir using a multi-chiroptical approach. Org Biomol Chem 13(10):2999–3010
13. Li Y, Lin Z, Guo M, Xia Y, Zhao M, Wang C, Xu T, Chen T, Zhu B (2017) Inhibitory activity of selenium nanoparticles functionalized with Oseltamivir on H1N1 influenza virus. Int J Nanomed 12:5733–5743
14. Hajzer V, Fišera R, Latika A, Durmis J, Kollár J, Frecer V, Tučeková Z, Miertuš S, Kostolanský F, Varečková E, Šebesta R (2017) Stereoisomers of Oseltamivir — synthesis, in silico prediction and biological evaluation. Org Biomol Chem 15:1828–1841
15. Willett DR, Rodriguez JD (2018) Quantitative Raman assays for on-site analysis of stockpiled drugs. Anal Chim Acta 1044:131–137
16. Eom G, Hwang A, Lee DK, Guk K, Moon J, Jeong J, Jung J, Kim B, Lim E-K, Kang T (2019) Superb specific, ultrasensitive, and rapid identification of the Oseltamivir-resistant H1N1 virus: naked-eye and SERS dual-mode assay using functional gold nanoparticles. ACS Appl Bio Mater 2:1233–1240
17. Eom G, Hwang A, Kim H, Yang S, Lee DK, Song S, Ha K, Jeong J, Jung J, Lim E-K, Kang T (2019) Diagnosis of Tamiflu-resistant influenza virus in human nasal fluid and saliva using surface-enhanced Raman scattering. ACS Sens 4(9):2282–2287
18. Li YH, Lin ZF, Zhao MQ et al (2016) Silver nanoparticle based codelivery of Oseltamivir to inhibit the activity of the H1N1 influenza virus through ROS-mediated signaling pathways. ACS Appl Mater Interfaces 8(37):24385–24393
19. Patel TS, Cinti S, Sun D, Li S, Luo R, Wen B, Gallagher BA, Stevenson JG (2017) Oseltamivir for pandemic influenza preparation: maximizing the use of an existing stockpile. Am J Infect Contr 45(3):303–305
20. Becke AD (1988) Density-functional exchange-energy approximation with correct asymptotic behavior. Phys Rev A 38:3098–3100
21. Lee C, Yang W, Parr RG (1988) Development of the Colle-Salvetti correlation-energy formula into a functional of the electron density. Phys Rev B 37:785–789
22. Pulay P, Fogarasi G, Pongor G, Boggs JE, Vargha A (1983) Combination of theoretical ab initio and experimental information to obtain reliable harmonic force constants Scaled quantum mechanical (QM) force fields for glyoxal acrolein butadiene formaldehyde and ethylene. J A Chem Soc 105:7073
23. Rauhut G, Pulay P (1995) Transferable scaling factors for density functional derived vibrational force fields. J Phys Chem 99:3093–3099
24. Rauhut G, Pulay P (1995) Transferable scaling factors for density functional derived vibrational force fields. J Phys Chem 99:14572
25. Sundius T (2002) Scaling of ab-initio force fields by MOLVIB. Vib Spectrosc 29:89–95
26. Miertus S, Scrocco E, Tomasi J (1981) Electrostatic interaction of a solute with a continuum. Chem Phys 55:117–129
27. Tomasi J, Persico J (1994) Molecular interactions in solution: an overview of methods based on continous distributions of the solvent. Chem Rev 94:2027–2094
28. Marenich AV (2009) Cramer CJ, Truhlar DG, Universal solvation model based on solute electron density and a continuum model of the solvent defined by the bulk dielectric constant and atomic surface tensions. J Phys Chem B 113:6378–6396
29. Karrouchi K, Brandán SA, Sert Y, El-marzouqi H, Radi S, Ferbinteanu M, Faouzi MEA, Garcia Y, Ansar M (2020) Synthesis X-ray structure Vibrational spectroscopy DFT investigation and biological evaluation studies of (E)-N'-(4-(dimethylamino) benzylidene)-5-methyl-1H-pyrazole-3-carbohydrazide. J Mol Struct 1219:128541
30. Karrouchi K, Brandán SA, Sert Y, El-marzouqi H, Radi S, Ferbinteanu M, Garcia Y, Ansar M (2021) Synthesis structural molecular docking and spectroscopic studies of (E)-N'-(4-methoxybenzylidene)-5-methyl-1H-pyrazole-3-carbohydrazide. J Mol Struct 1228:129714
31. El Kalai F, Karrouchi K, Baydere C, Daoui S, Allali M, Dege N, Benchat N, Brandán SA (2021) Synthesis crystal structure spectroscopic studies NBO AIM and SQMFF calculations of new pyridazinone derivative. J Mol Struct 1223:129213
32. Romano E, Issaoui N, Manzur ME, Brandán SA (2020) Properties and molecular docking of antiviral to COVID-19 chloroquine combining DFT calculations with SQMFF approach. International Journal of Current Advanced Research 9(8A):22862–22876
33. Romani D, Noureddine O, Issaoui N, Brandán SA (2020) Properties, reactivities and molecular docking of potential antiviral to treatment of COVID-19 niclosamide in different media. Biointerface Research in Applied Chemistry 10(6):7295–7328
34. Veber DF, Johnson SR, Cheng H-Y, Brian R, Ward KW, Kopple KD (2002) Molecular properties that influence the oral bioavailability of drug candidates. J Med Chem 45:2615–2623
35. Lipinski CA, Lombardo F, Dominy BW, Feeney PJ (2001) Experimental and computational approaches to estimate solubility and permeability in drug discovery and development setting. Adv Drug Deliv Rev 46:3–26
36. Romani D, Brandán SA (2019) Effect of the side chain on the properties from cidofovir to brincidofovir, an experimental

antiviral drug against to Ebola virus disease. Arab J Chem 12:2959–2972
37. Romani D, Márquez MJ, Márquez MB, Brandán SA (2015) Structural, topological and vibrational properties of an isothiazole derivatives series with antiviral activities. J Mol Struct 1100:279–289
38. Romani D, Brandán SA (2017) Investigating the structural and vibrational properties of the nucleoside reverse transcriptase inhibitor emtricitabine. International Journal of Science and Research (IJSR) 8:1
39. Brandán SA (2017) Structura topological electronic and vibrational properties of the antiviral trifluridine agent Their comparison with thymidine. Paripex A Indian Journal of Res 6(10):346–36
40. Romani D, Brandán SA (2017) Spectroscopic and structural study of the antiviral agent idoxuridine by using DFT and SCRF calculations. Int J Sci Res (IJSR) 8(1):66–86
41. Ladetto MF, Márquez MJ, Romani D, Brandán SA (2019) Structural and vibrational studies on isomers of antiviral ribavirin drug in gas and aqueous environmental by using the SQM approach. J Adv Chem 16:6325–6353
42. Iramain MA, Brandán SA (2018) Structural and vibrational study on the acid, hexa-hydrated and anhydrous trisodic salts of antiviral drug Foscarnet. Drug Des Int Prop Int J 1(3):1–17
43. Checa MA, Rudyk RA, Chamorro EE, Brandán SA, Chapter 1, Structural and vibrational properties of a reverse Inhibitor against the HIV Virus, Dideoxynucleoside Zalcitabine in gas and aqueous solution phases, pg. 1–26, Edited Collection, Nova Science Publishers, Inc. (2015).
44. Frisch J, Trucks GW, Schlegel HB, Scuseria GE, et al., Gaussian 09, Revision A.02, M. Gaussian, Inc., Wallingford CT, 2009.
45. Ugliengo P (1998) MOLDRAW Program. University of Torino, Dipartimento Chimica IFM, Torino, Italy
46. Glendening ED, Badenhoop JK, Reed AD, Carpenter JE, Weinhold F, NBO 3.1; Theoretical Chemistry Institute, University of Wisconsin; Madison, WI, 1996.
47. Bader RFW, Atoms in molecules, a quantum theory, Oxford University Press, Oxford, 1990, ISBN: 0198558651
48. Biegler-Köning F, Schönbohm J, Bayles D (2001) AIM2000; A program to analyze and visualize atoms in molecules. J Comput Chem 22:545
49. Besler BH (1990) Merz Jr, KM Kollman P, Atomic charges derived from semiempirical methods. J Comp Chem 11:431–439
50. Nielsen AB, Holder AJ, *Gauss View 5*.0, User's reference, GAUSSIAN Inc., Pittsburgh, PA, 2008.
51. Brandán SA (2021) Normal internal coordinates Force fields and vibrational study of species derived from antiviral adamantadine. Int J Quantum Chem 121(2):e26425
52. Ditchfield R (1974) Self-consistent perturbation theory of diamagnetism. I. A gage-invariant LCAO (linear combination of atomic orbitals) method for NMR chemical shifts. Mol Phys 27:714–722
53. Keresztury G, Holly S, Besenyei G, Varga J, Wang AY, Durig JR (1993) Vibrational spectra of monothiocarbamates-II IR and Raman spectra vibrational assignment conformational analysis and ab initio calculations of S-methyl-N N-dimethylthiocarbamate Spectrochim. Acta 49A:2007–2026
54. Górecki M (2015) (A configurational and conformational study of (−)-Oseltamivir using a multi-chiroptical Approach. Org Biomol Chem 13:2999
55. Naumov P, Yasuda N, Rabeh WM, Bernstein J (2013) (The elusive crystal structure of the neuraminidase inhibitor Tamiflu (Oseltamivir phosphate): molecular details of action. Chem Commun 49:1948–1950
56. Parr RG, Pearson RG (1983) Absolute hardness: companion parameter to absolute electronegativity. J Am Chem Soc 105:7512–7516